NeuroImage 248 (2022) 118867

Contents lists available at ScienceDirect

NeuroImage

journal homepage: www.elsevier.com/locate/neuroimage

Layer-specific activation in human primary somatosensory cortex during tactile temporal prediction error processing

Yinghua Yu[a,b,*], Laurentius Huber[c], Jiajia Yang[a,b], Masaki Fukunaga[d], Yuhui Chai[b], David C. Jangraw[b], Gang Chen[e], Daniel A. Handwerker[b], Peter J. Molfese[b], Yoshimichi Ejima[a], Norihiro Sadato[d], Jinglong Wu[a,f], Peter A. Bandettini[b,g]

[a] Graduate School of Interdisciplinary Science and Engineering in Health Systems, Okayama University, 3-1-1 Tsushima-Naka, Kita-ku, Okayama 700-8530, Japan
[b] Section on Functional Imaging Methods, National Institute of Mental Health, Building 10, 10 Center Dr Bethesda, MD 20892, USA
[c] MR-Methods Group, MBIC, Cognitive Neuroscience Department, Faculty of Psychology and Neuroscience, University of Maastricht, Cognitive Neuroscience, Room 1.014, Oxfordlaan 55, 6229 EV Maastricht, The Netherlands
[d] Division of Cerebral Research, National Institute for Physiological Sciences, 38 Nishigonaka, Myodaiji, Okazaki, Aichi, 444-8585 Japan
[e] Scientific and Statistical Computational Core, National Institute of Mental Health, Building 10, 10 Center Dr Bethesda, MD 20892, USA
[f] Beijing Institute of Technology, 5 South Zhongguancun Street, Hiadian District, Beijing 100081, China
[g] Functional MRI Core Facility, National Institute of Mental Health, Building 10, 10 Center Dr Bethesda, MD 20892, USA

ARTICLE INFO

Keywords:
Layer-specific fMRI
Tactile prediction
Primary somatosensory cortex
Temporal prediction error
High-resolution CBV–fMRI

ABSTRACT

The human brain continuously generates predictions of incoming sensory input and calculates corresponding prediction errors from the perceived inputs to update internal predictions. In human primary somatosensory cortex (area 3b), different cortical layers are involved in receiving the sensory input and generation of error signals. It remains unknown, however, how the layers in the human area 3b contribute to the temporal prediction error processing. To investigate prediction error representation in the area 3b across layers, we acquired layer-specific functional magnetic resonance imaging (fMRI) data at 7T from human area 3b during a task of index finger poking with no-delay, short-delay and long-delay touching sequences. We demonstrate that all three tasks increased activity in both superficial and deep layers of area 3b compared to the random sensory input. The fMRI signal was differentially modulated solely in the deep layers rather than the superficial layers of area 3b by the delay time. Compared with the no-delay stimuli, activity was greater in the deep layers of area 3b during the short-delay stimuli but lower during the long-delay stimuli. This difference activity features in the superficial and deep layers suggest distinct functional contributions of area 3b layers to tactile temporal prediction error processing. The functional segregation in area 3b across layers may reflect that the excitatory and inhibitory interplay in the sensory cortex contributions to flexible communication between cortical layers or between cortical areas.

1. Introduction

For survival in a changing environment, humans learn from experience to predict future events. Critical to this capacity is the interpretation of sensory input and the generation of internal prediction about future inputs (de Lange et al., 2018; Mumford, 1992; Shipp et al., 2013). For example, when humans perceive a rhythmic tactile sequence, they can take advantage of the temporal regularity to form predictions about the timing of future inputs (Yu et al., 2019). If these predictions match the temporal rhythms of actual sensory stimuli, this information can be used to enhance the perception of subsequent inputs. Alternatively, if an incoming signal does not match the prediction (e.g., occurs later than predicted), the brain will generate prediction error signals that can be used to update the internal prediction, thereby improving future sensory perception. This process is achieved within hierarchically organized cortical structures in which higher-level areas generate predictions and transmit signals back to lower-level areas through top-down connections. In contrast, lower-level areas serve to calculate prediction errors between prediction and actuality and then transmit error signals back to higher-level areas through bottom-up connections to optimize internal prediction (Barrett and Simmons, 2015; Keller and Mrsic-Flogel, 2018). The human primary somatosensory cortex (S1) is essential not only for receiving sensory input but also for receiving predictive feedback (Yu et al., 2019), but the precise functions of individual cortical layers of S1 in prediction error processing is unclear.

The neural circuits underlying tactile prediction processing have been mapped to area 3b of human S1. In our previous study (Yu et al.,

* Corresponding author.
E-mail address: yinghua.yyh@gmail.com (Y. Yu).

https://doi.org/10.1016/j.neuroimage.2021.118867.
Received 21 July 2021; Received in revised form 27 December 2021; Accepted 29 December 2021
Available online 30 December 2021.

2019), we demonstrated that specific layers in area 3b are specialized for receiving sensory information and predictive feedback. Specifically, we found that the sensory inputs preferentially terminate in the middle cortical layer 4 (L4), whereas the top-down predictive feedback from higher-level areas project to superficial layers 2/3 (L2/3) and deep layers 5/6 (L5/6). Through these top-down pathways, superficial and deep layers received modulatory input for sensory prediction even in the absence of actual sensory inputs. Furthermore, anatomical and physiological studies on non-human animals (Constantinople and Bruno, 2013; Quiquempoix et al., 2018) indicate that L2/3 and L5/6 neurons receive direct inputs from L4 neurons, thus serving a secondary function in cortical processing of feedforward inputs. L2/3 pyramidal neurons are critical for receiving top-down signals from higher-level areas, whereas interlaminar links within L2/3 and L5/6 neurons support the temporal integration of feedforward and feedback signals for predicting future sensations (Kachergis et al., 2014; Manita et al., 2015; Quiquempoix et al., 2018; Roelfsema and Holtmaat, 2018; Thomson, 2007). Therefore, L2/3 and L5/6 neurons are critical for integrating information related to sensory input with cortical feedback to reduce prediction errors.

Recent computational modeling studies have proposed that L2/3 and L5/6 neurons make distinct functional contributions to sensory prediction and prediction error processing (Barrett and Simmons, 2015; Bastos et al., 2012). L2/3 pyramidal neurons are thought to compute the error between predicted and actual sensory inputs and then send error signals to higher-level areas (e.g., middle cingulate cortex (Yang et al., 2021a)) and to L5/6 neurons in the same column. The cortico-cortical connections from L2/3 neurons to higher-level areas serve to transmit prediction error signals so that these areas can generate more accurate future predictions. In contrast, the intracolumnar projections from L2/3 to L5/6 modulate the gain of incoming sensory input strength (Barrett and Simmons, 2015). These distinct functional roles of L2/3 and L5/6 neurons are consistent with those reported in animal studies (Jordan and Keller, 2020; O'Connor et al., 2010; Pluta et al., 2015; Quiquempoix et al., 2018). In particular, a recent study (Jordan and Keller, 2020) suggests that L2/3 neurons of the mouse visual cortex compute prediction errors by subtracting predicted and actual visual flow inputs, whereas L5/6 neurons play a role in integrating visual flow and locomotion. To date, however, there is no empirical evidence for such precise contributions of L2/3 and L5/6 to prediction and prediction error in humans. This lack of knowledge is largely due to the technical challenges of capturing layer-specific brain activity in the relatively thin (about 2 mm) human sensory cortex (Dumoulin et al., 2018; Finn et al., 2020; Self et al., 2019; Turner and De Haan, 2017; Uludağ and Blinder, 2018; Yang et al., 2021b).

In the present study, we aim to investigate the cortical layer-specific activity that is related to prediction error processing in human area 3b. We employed layer-specific functional magnetic resonance imaging (fMRI) at 7T using concurrent measures of vascular-space-occupancy (VASO) and blood oxygenation level-dependent (BOLD) imaging (Huber et al., 2020, 2017, 2016). Following the perspective of the previous findings (Jordan and Keller, 2020), we hypothesize that both L2/3 and L5/6 of human area 3b will be involved in the prediction error processing, while each layer may have distinct functions. In particular, L2/3 might receive the top-down feedback and feature for error calculation, while the L5/6 might specialize in the integration and modulation of multiple inputs such as incoming sensory input and top-down feedback. To test this hypothesis, we designed three tactile temporal prediction (TP) tasks. All participants received rhythmic tactile finger poking in three TP tasks and were asked to predict a target poke to the index finger. We manipulated the target timing such that index finger poking occurred either on-beat (TPon task – no delay) or off-beat (TPoff task – delayed). The violation of the temporal rhythm in the off-beat task is referred to as prediction error condition, which allowed us to investigate how the prediction error processing modulates the activity of L2/3 and L5/6 within area 3b. For the off-beat TPoff task, we further manipulated the length of the temporal interval before the index finger poking (i.e., TPoff_short task - delayed by a one beat interval; TPoff_long task – delayed by a two beats interval). A long interval is expected to engage an inhibitory process (Klein and Ivanoff, 2000; Nobre and Van Ede, 2018) to affect the activity in the sensory cortex, which allowed us to investigate how the extended off-beat delay period affects the activity of L2/3 and L5/6 within area 3b.

2. Materials and methods

2.1. Human participants

Eleven healthy right-handed volunteers (5 males and 6 females; age range 21–38 years) participated in the fMRI experiments. Six of them participated after providing informed consent to a protocol approved by the National Institutes of Health Combined Neuroscience Institutional Review Board (93-M-0170, ClinicalTrials.gov identifier: NCT00001360) in accordance with the Belmont Report and U.S. Federal Regulations protecting human subjects. Additional five participants gave written informed consent under the local medical ethics committee at the National Institute for Physiological Sciences, Japan. One female was re-invited to participate in an additional session (on a different day) to confirm reproducibility; therefore, twelve experimental sessions (n = 12) were conducted in total.

2.2. Experimental session setup and image acquisition

Each session consisted of one finger somatotopic mapping run of 9.9 min duration and one or two prediction task runs of 16 min duration. No participant was in the scanner for longer than 120 min per session.

The same fMRI sequence and image reconstruction pipeline was used as in our previous study (Yu et al., 2019). Slice-selective slab-inversion concurrent measures of VASO (Lu et al., 2003) and BOLD signals were acquired using a 7T scanner (Siemens Healthineers, Erlangen, Germany) equipped with a 32-channel RF coil (Nova Medical, Wilmington, MA, USA) and an SC72 body gradient coil. The VASO-relevant TR-loop acquisition settings were as follows: $TI1_{nulled}$ = 1100 ms, $TI2_{BOLD}$ = 2845 ms, and TR_{pair}= 3490 ms. The coil-combined data comprised interleaved BOLD and VASO contrasts obtained as concomitant time series (Huber et al., 2017). These time series are corrected for rigid volume motion and are separated by contrast with the effective temporal resolution of TR = 3490 ms for each individual contrast. The nominal resolution was 0.71 mm across cortical depths with 1.8-mm thick slices perpendicular to the postcentral bank of the right central sulcus with 3D-EPI (Poser et al., 2010). VASO contrast is corrected for BOLD contaminations by the division of blood nulled MR-signal and not-nulled MR-signal across consecutive TRs. This was performed based on 1–4 short EPI test runs with 5 measurements and their online depiction in the vendor-provided 3D-viewer. The higher detection sensitivity of BOLD (with low layer specificity) was used to determine the single-voxel activity scores for subsequence regions of interest (ROI) definition. The higher layer specificity of VASO (with lower sensitivity) was used to extract layer-profiles of voxel-averages for each layer without venous biases.

2.3. Experimental paradigm and procedures

2.3.1. Finger somatotopic mapping run

To delineate the precise cortical ROI for individual participants, we mapped the somatotopic representation of the left four fingers (D2: index, D3: middle, D4: ring, and D5: pinky) in the contralateral area 3b using an on–off block design. A custom-designed finger stimulation device (Yu et al., 2019) was used to poke each finger through the plastic sticks under each fingertip. During on-phase (17.5 s), each of the four fingers was randomly and independently poked at 4–5 Hz and each finger was poked five times in one run. Participants were instructed with

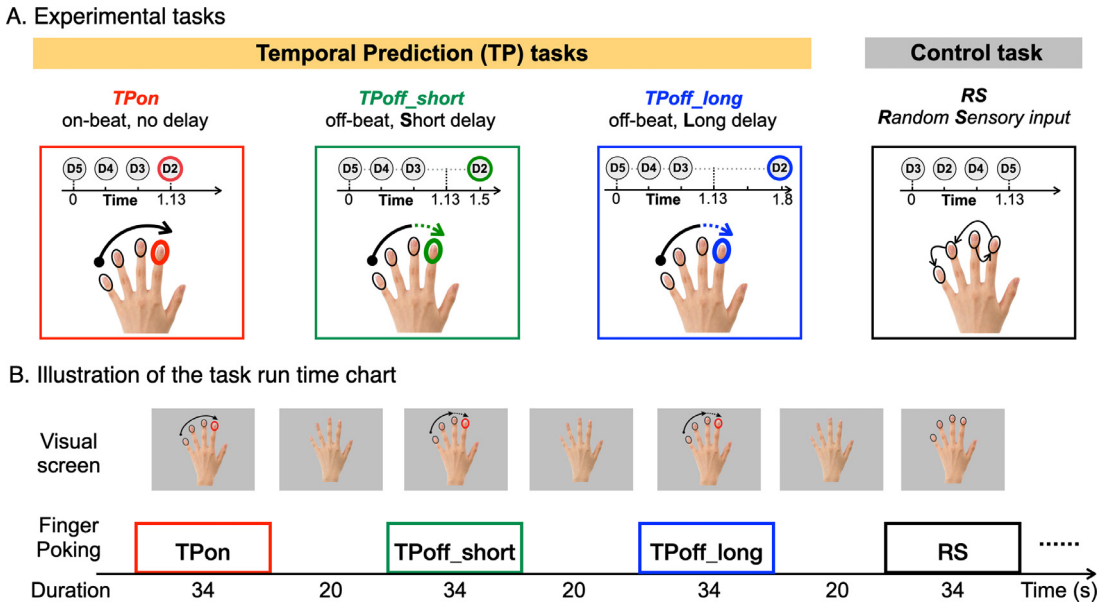

Fig. 1. Illustration of the experimental tasks and time chart. (A) Tactile stimulation sequences of the three temporal prediction (TP) tasks and the random sensory (RS) input control task. In the three TP tasks, the fingers were stimulated in set order (pinky to index), with the index finger receiving stimulation with the same interval as the other fingers (on-beat). In the TPoff_short and TPoff_long tasks, index finger stimulation was delayed by one beat (approximately 0.37 s) or by two beats (approximately 0.74 s), respectively. In the RS task, fingers were stimulated in a random order. (B) The four task blocks were presented for 34 s at 20 s intervals, and each task block was repeated four times in each run. The order of the blocks was counterbalanced. TPon: Temporal Prediction on-beat, no delay; TPoff_short: Temporal Prediction off-beat, short delay; TPoff_long: Temporal Prediction off-beat, long delay; RS: Random sensory input across four fingers.

the request: "Keep your attention on the left poked fingertips during on-phase." Due to time limitations, one of the eleven participtants performed somatotopic mapping run only for D2 and D3.

2.3.2. Tactile temporal prediction (TP) task run

In the following experiments, we investigated prediction and prediction error-induced signals across cortical layers during a rhythmic tactile stimulation task. As shown in **Fig. 1A**, participants received sequences of tactile pokes to the four fingertips in two general patterns: (a) & (b) sequentially from the pinky to index (D5 to D2) in the three TP tasks; (c) randomly poking across the four fingers in the random sensory (RS) input control task. In the TP tasks, the interval between stimulation of the pinky, ring, and middle fingers was held constant (at approximately 0.37 s), whereas the interval between the middle and index fingers was varied.

(a) Tactile temporal prediction on-beat (TPon) task: The participants were instructed with the following text on the screen: "Pay attention to the poking on each finger and then predict when your left index finger will be poked based on the temporal rhythm." The actual sensory stimuli involved the experimenter poking the participants' four fingers in an ordered fashion from D5 to D4 to D3 to D2. The temporal rhythm between each poking was approximately 0.37 s. In this case, the temporal rhythm of D2 poking matched the predicted rhythm learned from isochronous poking of the first three fingers. We expected that these learned rhythmic modulations would generate predictive feedback signals to the D2 region of area 3b. Thus, prediction of the D2 stimulus would improve by a consistent temporal relation.

(b) Tactile temporal prediction off-beat (TPoff_short and TPoff_long) tasks: The experimental instruction was the same as the TPon task. The actual sensory stimuli involved the experimenter poking the four fingers of the participant in an ordered fashion from D5 to D4 to D3 to D2. The temporal rhythm between each poking from D5 to D3 was approximately 0.37 s. However, the last poking D2 was delayed by a one beat interval (additional 0.37 s) for TPoff_short task and two-beats interval (additional 0.74 s) for TPoff_long task. In these cases, the temporal rhythm of D2 poking mismatched the predicted rhythm learned from isochronous poking of the first three fingers. Thus, we expected that a longer D3-to-D2 stimulus interval would induce prediction errors manifested by distinct layer-specific activity patterns in the D2 region of area 3b.

(c) Random sensory (RS) input control task: The participants were instructed with the following text on the screen: "Pay attention to the poking on each finger, but do not try to predict any pattern." Even we cannot rule fully out the prediction effects since humans are keeping predict the future inputs based on the predictive coding principle (Bastos et al., 2012; de Lange et al., 2018), it was expected to reduce the prediction of the next poking position by presenting the finger poking in random order. Thus, the RS task was used to induce thalamic input to the D2 region in area 3b with reduced stimulus-driven prediction.

As shown in **Fig. 1B**, all four task blocks were delivered for 34-s separated by a 20-s off period, and each task block was usually repeated four times. The order of the blocks was counterbalanced. Furthermore, to prevent adaptation, TPoff_short and TPoff_long blocks included 80% delayed poking trials, and 20% of trials included rhythmic poking as TPon task. By adding 20% no-delay (TPon) trials to TPoff blocks, the amount of error components in the TPoff blocks was varied but still more significant than TPon blocks. Thus, the TPoff vs. TPon contrast was expected to reflect the change in activity in layers that are more responsive to prediction error processing.

2.4. Data analysis

2.4.1. Motion correction

All fMRI data were corrected for head motion using Statistical Parametric Mapping Version 12 software (Functional Imaging Laboratory, University College London, UK) (Friston et al., 2007). To minimize errors on the motion estimation due to non-linear motion at air-tissue interfaces, the motion parameter estimation was restricted to a manually drawn ROI of the central sulcus.

2.4.2. Anatomical reference methods

To avoid additional resolution loss due to repeated resampling steps and to avoid any errors of the distortion correction and registration, we

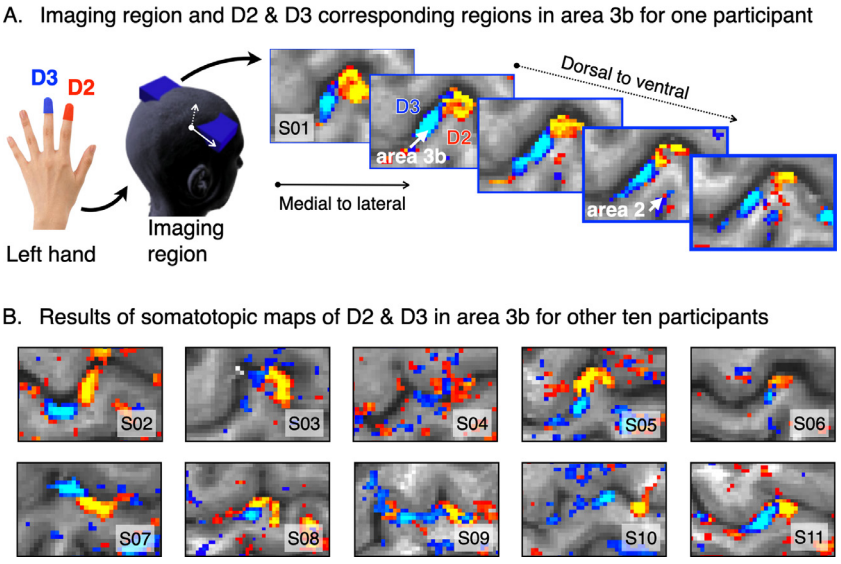

Fig. 2. Somatotopic mapping of area 3b representing the index finger (D2) and middle finger (D3) for all participants. (A) Imaging region and finger somatotopic map of one participant. Tactile poking of the participant's left index and middle fingers induced clear activation along the contralateral (right hemisphere) area 3b. (B) Sample somatotopic maps of D2 and D3 finger representations for other ten participants. The finger-specific activation hotspots shown here were used to determine the ROIs for the extraction of layer profiles. Note that the depicted data refer to the BOLD contrast.

did not register the functional data to an anatomical reference dataset. Instead, we used the functional data directly as an anatomical reference as was performed previously (Yu et al., 2019).

2.4.3. General linear model (GLM) analysis

GLM was conducted using FSL5.0.9 (FMRIB Software Library, University of Oxford, UK) (Jenkinson et al., 2012). VASO and BOLD signals for all runs were modeled with a BLOCK function convolved with the canonical hemodynamic response function using the FEAT tool of FSL. Furthermore, we also used several AFNI commands (Version ID = AFNI_18.1.08) for fMRI data processing (Cox, 1996).

2.4.4. Layering methods and profile extraction

Layer-specific analyses were conducted using the open software suite LAYNII (https://github.com/layerfMRI/LAYNII) (Huber et al., 2021). The borderlines between cerebrospinal fluid (CSF), gray matter (GM), and white matter (WM) were used as the basis to define cortical depths (a.k.a. layers). To avoid singularities at the edges in angular voxel space, the cortical depths were defined on a five-fold finer grid than the original EPI resolution. Then, we first create the finger ROI images contain the segmentation of GM and its borders, which consists of four integer values (0 = irrelevant voxels, 1 = inner GM surface voxels, 2 = outer GM surface voxels, 3 = pure GM voxels). By applying the layer classification command to these ROI images, 11 equi-volume lines (Waehnert et al., 2014) were calculated across the cortical depth in each ROI. These ROIs were used to extract the cortical depth-dependent profiles of all experimental tasks. Please note that with a nominal 0.71 mm resolution and an approximate cortical thickness of 2 mm in area 3b, the effective resolution allows the detection of only 3 independent data points. Hence, the defined 11 cortical depths do not represent the MRI effective resolution. For visualization, cortical layer-specific smoothing was applied. However, all cortical activity profiles were evaluated from the unsmoothed data.

2.4.5. Statistical analysis

The difference between any pair of task conditions were statistically assessed through a linear mixed-effects (LME) modeling approach using the R package nlme (R Core Team, 2013). With the pair-wise difference at each layer from each participant as the data for the response variable, the LME model was formulated with no intercept, with layers as a fixed-effects factor and with a random intercept for cross-sessions variability.

3. Results

3.1. Finger somatotopic mapping run

The finger regions in area 3b were somatotopically mapped in this run, in which fingers were separately poked. The examples of index finger (D2, red) and middle finger (D3, blue) BOLD activation map of one participant is presented in **Fig. 2A**. A clear representation of D2 and D3 fingers from the medial to lateral side was identified along area 3b in all participants (**Fig. 2B**). These maps were subsequently used to determine the ROIs of each finger in relevant parts of area 3b during the TP and RS task runs. To reduce the overlap effect of adjacent fingers representation in area 3b, we delineate the precise D2 ROI by avoiding overlapping voxels with other fingers.

3.2. Temporal prediction (TP) and random sensory (RS) input control task runs

We examined the functional activity in area 3b during three TP tasks and compared them to those of a RS task (**Fig. 3AB**). Spatial maps of results (shown for a representative participant in **Fig. 3B**) indicate that all four tasks excite area 3b, which is consistent with our previous finding (Yu et al., 2019).

Averaged layer-specific VASO and BOLD response profiles in the D2 ROI are shown for all four tasks in **Fig. 4A**. These VASO activity profiles were highly consistent with the activity map for a single participant shown in **Fig. 3B**. Despite residual inter-participant variability, the response profiles for all participants are almost consistently modulated for the different tasks. Specifically, the TP tasks increased activity in the superficial layers regardless of prediction error (VASO profiles in **Fig. 4B**). However, activity in the deep layers of area 3b differed across the three TP tasks. Specifically, activity in deep layers increased during the TPoff_short task (green dashed line) compared with during the TPon task, but during the TPon and TPoff_long tasks did not differ significantly (blue dashed line). In contrast to all TP tasks, the non-prediction RS task evoked strong activity in the middle layers but not in superficial or deep layers (black dashed line in **Fig. 4A**). Since the modulation of prediction error activity was designed for D2, the activity of other finger ROIs (i.e., D3, D4, D5) showed mostly similar patterns across tasks which all tasks evoked the most robust activity in the middle layers. In contrast, we can confirm task-related differences from the BOLD responses, but the distinction between layers was less clear. This is because BOLD has limited layer specificity and is biased toward the superficial layers and

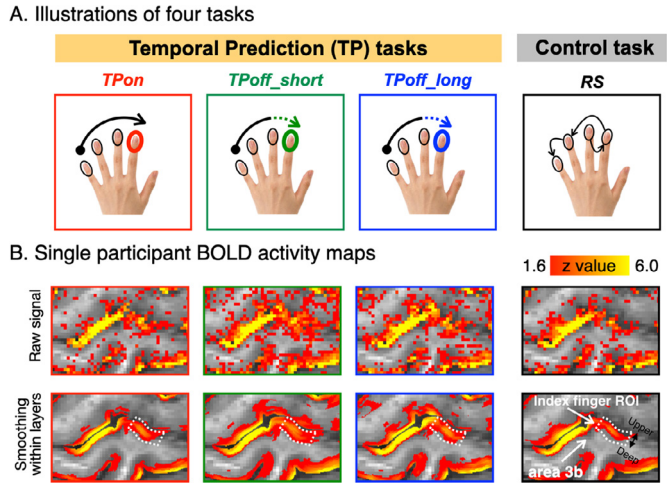

Fig. 3. Illustration of the experimental tasks and the corresponding BOLD activation maps of a representative participant. (A) Tactile stimulation sequences of the three temporal prediction (TP) tasks and the random sensory (RS) input control task. (B) Activation maps (FSL z statistic maps, clusters determined by $z > 1.6$) during the four tasks. Top row: raw data, Bottom row: with smoothing in each layer. The white dashed line demarcates the region of interest for the index finger representation in area 3b. All three TP tasks evoked strong activity in both superficial and deep layers regardless of whether a prediction error was present. In contrast, the RS task evoked more robust activity in the middle layers.

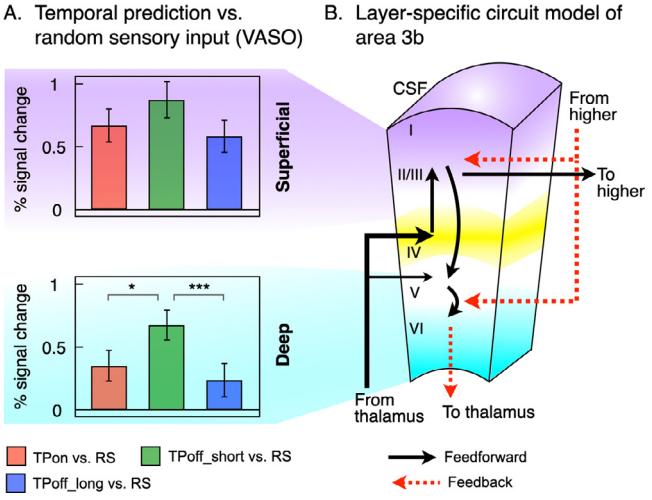

Fig. 5. Averaged VASO signal changes in superficial and deep layers of human cortical area 3b and a layer-specific circuit model. (A) The bar graphs represent the average activity changes in superficial layers (cortical depths 2–4 in Fig. 3) and deep layers (cortical depths 7–10) for all sessions. (B) A layer-specific circuit model of the primary somatosensory cortex (area 3b). *: $p < 0.05$, ***: $p < 0.001$.

large draining veins. Furthermore, we performed an additional analysis to verify whether the different finger stimulation sequences (TPon and TPoff tasks versus RS task) affect the steady-state functional response over the blocks. In short, we did not find any specific functional response pattern for the RS task compared to other prediction tasks (Figures s1 and s2). The analysis processing and results are provided in the Supplementary material. Notably, the more finely defined 11 cortical depths (data points) do not represent the effective resolution in our MRI data.

To quantify the layer-specific prediction and prediction error activity in superficial and deep layers of area 3b, we collected data points from superficial layers (data points 2–4) and deep layers (data points 7–10) and compared VASO signal changes among the three TP tasks and RS task (**Fig. 5A**). These contrasts revealed inverted V-shaped activity in the deep layers that was dependent on the length of the delay between middle and index finger poking, with enhanced activity in the deep layers during the short delay period [TPoff_short vs. TPon, effect magnitude = 0.32±0.09, $p = 0.01$] but reduced again during the longer delay period [TPoff_long vs. TPoff_short, effect magnitude = 0.43±0.09, $p < 0.001$]. Again, activity in deep layers during

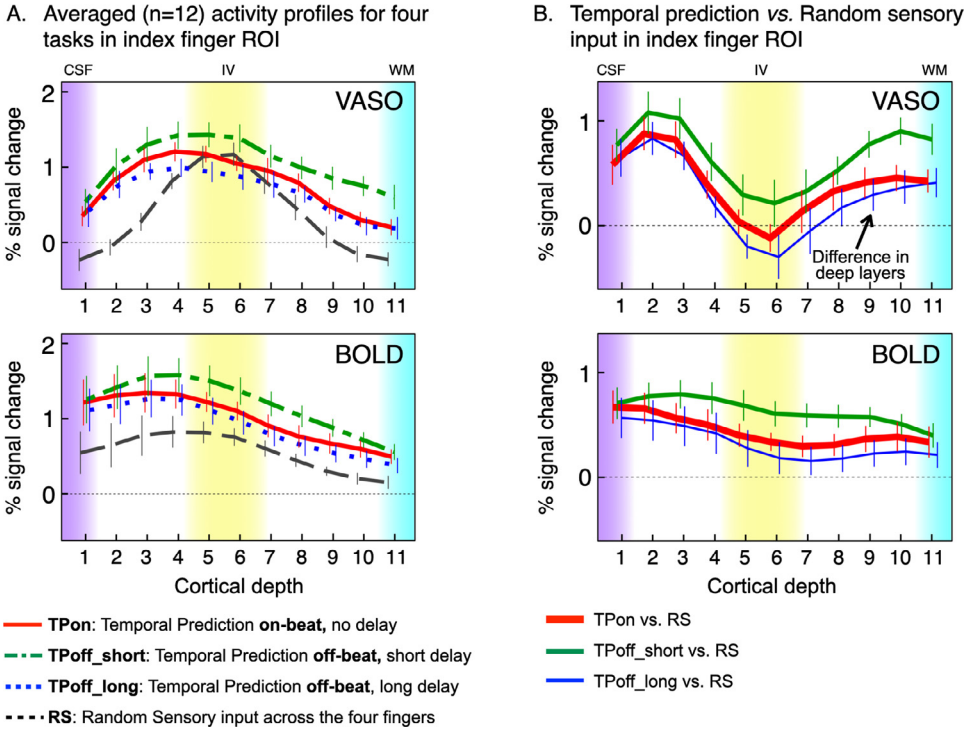

Fig. 4. Layer-specific VASO and BOLD activity profiles of the index finger region in contralateral area 3b. (A) Four tasks differentially modulated even both VASO and BOLD activity profiles, the distinction between layers of BOLD activity was less clear. (B) The VASO activity profiles show that for all three TP tasks compared to the RS task, the activation increased to the same level in superficial layers (left) but differentially in the deep layers (right). The TPoff_short task (green line) induced the strongest activation in the deep layers than the other two TP tasks. Here, $n = 12$ represents the number of individually conducted experimental session (eleven participants with one retest). Error bars indicate the standard error of the mean across sessions.

the TPon and TPoff_long tasks did not differ significantly [effect magnitude = 0.11±0.09, p = 0.792]. Thus, activity in the deep layers was enhanced by temporal prediction errors in the TPoff_short task, but these laminar effects were inhibited when the stimulation was delayed for a longer time (i.e., TPoff_long task). In contrast, there were no differences in superficial layers activity among these three TP tasks (all p values > 0.365).

4. Discussion

Prediction error processing is a crucial part of adapting to changing conditions. However, it remains unclear how prediction error processing is implemented in sensory cortical layers. In the present study, we designed one TPon task with rhythmic poking from left pinky to index finger and two TPoff tasks that are expected to engage the prediction error processing by manipulating the poking interval between the left middle and index finger (TPoff_short – delayed by a one beat interval, TPoff_long – delayed by a two beats interval). We showed distinct layer-specific activity in human area 3b (**Fig. 4AB**) during three prediction tasks by using high-resolution fMRI at 7T. By comparing layer-specific activity in area 3b during the three TP tasks, we showed that activity in deep layers (L5/6) is selectively modulated by the error processing which occurred during the delayed period of the TPoff_short task, while superficial layers (L2/3) showed comparable activity during all TP tasks (**Fig. 5A**). Our findings of the distinct layer profiles are roughly consistent with our hypothesis that both superficial and deep layers of human area 3b will be involved in the prediction error processing while each layer contribute to distinct parts of this processing.

The distinct activity profiles across cortical layers in **Fig. 4B** showed that prediction and prediction error processing produce specific laminar patterns of neural activity in the sensory cortex. We included the RS task as a control to characterize the layer-specific activity of sensory input without prediction and prediction error. We identified one peak of activity in the middle layers (L4) of area 3b for the RS task (VASO signals, dashed black line, **Fig. 4A**), which is supported by the understanding that the middle layer of the primary sensory cortex receives thalamic sensory inputs (Douglas and Martin, 2004). Nevertheless, one would expect to observe more robust activity than we found in both superficial and deep layers during the RS task, which might be caused by the basic sensory processing. That is, even though participants were asked not to predict any pattern in the RS task, it is likely that this activity cannot be consciously suppressed: the predictive coding principle (Bastos et al., 2012; de Lange et al., 2018) suggests that this instinct is deeply ingrained. These predictive signals are thought to increase the activity in both superficial and deep layers. One possible explanation of the decreased activity in the superficial and deep layers in the present study is that cross-finger suppression in area 3b occurred as all participants' four fingers were poked during the RS task. This cross-finger suppression effect in area 3b has been confirmed in non-human primates (Reed et al., 2011, 2010) by stimulating two hand locations simultaneously or asynchronously. They found that the response suppression on the adjacent fingers in area 3b neurons occurred for asynchrony adjacent fingers stimulation, but the maximum suppression effect occurred at the stimulus interval of 30 ms and almost equally for all other longer intervals (up to 500 ms). In the present study, given all the intervals between the D3 and D2 stimulation are greater than 375 ms, we believe that this cross-finger suppression plays a negligible contribution to our temporal prediction findings.

The direct comparison of the TPon and TPoff_short tasks to the RS task provided the evidence to support our hypothesis that both superficial and deep layers of human area 3b are involved in prediction error processing. Specifically, while both TPon and TPoff_short tasks increased activity in superficial and deep layers compared to the RS task, activity in deep layers was further strengthened by prediction errors in the TPoff_short task. This enhanced activity within the deep layers may reflect the occurrence of predictive feedback and prediction error (**Fig. 5A**). These results are consistent with our previous layer-specific fMRI findings of top-down feedback input to the superficial and deep layers of area 3b (Yu et al., 2019) and of layer-specific findings from the visual modality (Lawrence et al., 2018). Beyond these previous studies, the present study showed that deep layers' activation during the TPoff_short task could represent a distinct function in prediction error processing. Assuming that the amplitude of prediction error is encoded in deep layers (Kanai et al., 2015a), the prediction error signals could be integrated with predictive feedback from high-level areas to inform posterior expectations about tactile perception.

Intriguingly, we found that the increased deep layers activity observed in the TPoff_short task was reduced by extending the off-beat interval in the TPoff_long task (**Fig. 5A**). This reduced fMRI signal in deep layers was thought to reflect the inhibitory neural activity (Fracasso et al., 2018; Huber et al., 2014) during the TPoff_long task. This phenomenon seems inconsistent with the previous findings that the off-beat event during rhythm-based prediction results in larger behavioral costs and increased brain activity for violation of prediction (Kanai et al., 2015b; Lee and Mumford, 2003; Rao and Ballard, 1999). One possible interpretation is that inhibitory processing may dominate during the longer delay period (TPoff_long task) when presenting targets outside the expected temporal window, thereby mitigating enhanced deep layers activity from the prediction error. In this context, in the present study, such inverted V-shaped activity characteristics (**Fig. 5A**) might reflect the recruitment of deep layers' excitatory neurons by prediction error encoding depending on the temporal window during this dynamic process. This "temporal tuning" of deep layers activity may enhance the fidelity of sensory prediction, allowing flexible regulation of sensory expectations at different temporal scales.

The most straightforward functional interpretation of this inhibition of deep layers' activity is preparation for a stimulus that then fails to arrive within the expected temporal window (Adesnik, 2018; Pluta et al., 2015, 2019; Slater et al., 2019). Given the nature of the TPoff_long task, feedforward connections rather than feedback connections may predominate. In other words, there are no top-down predictions to explain responses in lower sensory areas, but there are inhibitory mechanisms to prepare for new bottom-up inputs. These shifts lead to disinhibition of superficial layers and inhibition of deep layers. Previous non-human animal studies have suggested that excitatory and inhibitory interplay in deep layers contribute to flexible communication between cortical layers or between cortical areas (Adesnik, 2018; Harris and Mrsic-Flogel, 2013). Consistent with these studies, our findings suggest dominating inhibitory activity in deep layers of the human sensory cortex during longer prediction periods. Further, these findings demonstrate a simple and general mechanism in which prediction interacts with temporal preparative processing (at least within a certain temporal range) to influence perception. We speculate that time-dependent excitatory and inhibitory modulations in deep layers are critical for temporal prediction.

Our findings also provide insight into the temporal dynamics of inhibitory connectivity across areas and/or layers. Deep cortical layers communicate widely with target areas via both thalamocortical and intracortical connections (Slater et al., 2019). The canonical laminar organization includes excitatory feedforward inputs from the thalamus that project dominantly into L4 but also into L5 and L2/3 (**Fig. 5B**) (Constantinople and Bruno, 2013). Further, L2/3 provides feedforward input to both high-level areas and to L5/6, which in turn provides feedback to the thalamus and projects to L2/3, forming a complete loop (Adesnik and Naka, 2018). In contrast, other distinct inhibitory circuits may suppress activation in deep layers for processes such as adaptation (Mease et al., 2014). One potential neural mechanism for suppression of deep layers' activity in area 3b is through thalamocortical connections (Slater et al., 2019) during preparation for a predicted stimulus. Briefly, thalamocortical projections can carry excitatory signals to feedforward input layers when actual sensory stimulation occurs, whereas feedback inhibitory connections may progressively dominate when ac-

tual sensory input is delayed. Such reciprocal inhibitory connectivity may differentially modulate up- and downstream communication in response to temporal input patterns.

In summary, we used a well-established prediction task to investigate how a mismatch between expected and actual temporal sensory input (an error signal) modulates layer-specific activity in the primary somatosensory cortex. By manipulating the interval before an expected rhythmic stimulus to produce a time-dependent prediction error, we revealed distinct laminar activation patterns in the human cortical area 3b for prediction and prediction error tasks. These observations suggest layer-specific contributions to sensory prediction and prediction error processes as well as provide new insights into how the brain generates sensory-guided predictions. Moreover, we should point out that we took advantage of the high layer specificity of VASO to measure layer-specific activity in area 3b; however, the sensitivity of VASO is still low. This technical limitation resulted in the on-off block design, which may increase the block-wise bias and weaken the task effect. The current layer fMRI technique is becoming easier to use (Bandettini et al., 2021); future studies will focus on variation of temporal prediction processing across areas and layers with an event-related design.

Data and Code Availability

The data presented here are available from the corresponding author, Y.Y., upon reasonable request.

Credit authorship contribution statement

Yinghua Yu: Conceptualization, Methodology, Formal analysis, Investigation, Writing – original draft, Writing – review & editing. **Laurentius Huber:** Methodology, Formal analysis, Investigation, Writing – review & editing. **Jiajia Yang:** Conceptualization, Methodology, Formal analysis, Writing – review & editing. **Masaki Fukunaga:** Investigation. **Yuhui Chai:** Investigation. **David C. Jangraw:** Writing – review & editing. **Gang Chen:** Formal analysis. **Daniel A. Handwerker:** Writing – review & editing. **Peter J. Molfese:** Writing – review & editing. **Yoshimichi Ejima:** Writing – review & editing. **Norihiro Sadato:** Writing – review & editing. **Jinglong Wu:** Writing – review & editing. **Peter A. Bandettini:** Conceptualization, Supervision, Writing – review & editing.

Acknowledgments

We thank Arman Khojandi and Kenny Chung for support in human volunteer scanning. The research was conducted as part of the NIMH Intramural Research Program (#ZIA- MH002783). Funding: This work was supported by JSPS KAKENHI (JP18K15339, JP18H01411 and JP20K07722) and JST FOREST Program (JPMJFR2041) as well as Japan–U.S. Science and Technology Cooperation Program (Brain Research). Laurentius Huber was funded by the NWO VENI project 016.Veni.198.032.

Supplementary materials

Supplementary material associated with this article can be found, in the online version, at doi:10.1016/j.neuroimage.2021.118867.

References

Adesnik, H., 2018. Layer-specific excitation/inhibition balances during neuronal synchronization in the visual cortex. J. Physiol. 596, 1639–1657. doi:10.1113/JP274986.

Adesnik, H., Naka, A., 2018. Cracking the function of layers in the sensory cortex. Neuron 100, 1028–1043. doi:10.1016/j.neuron.2018.10.032.

Bandettini, P.A., Huber, L., Finn, E.S., 2021. Challenges and opportunities of mesoscopic brain mapping with fMRI. Curr. Opin. Behav. Sci. 40, 189–200.

Barrett, L.F., Simmons, W.K., 2015. Interoceptive predictions in the brain. Nat. Rev. Neurosci. 16, 419–429. doi:10.1038/nrn3950.

Bastos, A.M., Usrey, W.M., Adams, R.A., Mangun, G.R., Fries, P., Friston, K.J., 2012. Canonical microcircuits for predictive coding. Neuron 76, 695–711. doi:10.1016/j.neuron.2012.10.038.

Constantinople, C.M., Bruno, R.M., 2013. Deep Cortical Layers Are Activated Directly by Thalamus. Science (80-.). 340, 1591–1594. 10.1126/science.1236425

Cox, R.W., 1996. AFNI: software for analysis and visualization of functional magnetic resonance neuroimages. Comput. Biomed. Res. 29, 162–173. doi:10.1006/cbmr.1996.0014.

de Lange, F.P., Heilbron, M., Kok, P., 2018. How do expectations shape perception? Trends Cogn. Sci. 22, 764–779. doi:10.1016/j.tics.2018.06.002.

Douglas, R.J., Martin, K.A.C., 2004. Neuronal circuits of the neocortex. Annu. Rev. Neurosci. 27, 419–451. doi:10.1146/annurev.neuro.27.070203.144152.

Dumoulin, S.O., Fracasso, A., van der Zwaag, W., Siero, J.C.W., Petridou, N., 2018. Ultra-high field MRI: advancing systems neuroscience towards mesoscopic human brain function. Neuroimage 168, 345–357. doi:10.1016/j.neuroimage.2017.01.028.

Finn, E.S., Huber, L., Bandettini, P.A., 2020. Higher and deeper: bringing layer fMRI to association cortex. Prog. Neurobiol. 101930. doi:10.1016/j.pneurobio.2020.101930.

Fracasso, A., Luijten, P.R., Dumoulin, S.O., Petridou, N., 2018. Laminar imaging of positive and negative BOLD in human visual cortex at 7 T. Neuroimage 164, 100–111. doi:10.1016/j.neuroimage.2017.02.038.

Friston, K.J., Ashburner, J.T., Kiebel, S.J., Nichols, T.E., Penny, W.D., 2007. Statistical parametric mapping: the analysis of functional brain images, statistical parametric mapping the analysis of functional brain images.

Harris, K.D., Mrsic-Flogel, T.D., 2013. Cortical connectivity and sensory coding. Nature 503, 51–58. doi:10.1038/nature12654.

Huber, L.(Renzo), Poser, B.A., Bandettini, P.A., Arora, K., Wagstyl, K., Cho, S., Goense, J., Nothnagel, N., Morgan, A.T., van den Hurk, J., Müller, A.K., Reynolds, R.C., Glen, D.R., Goebel, R., Gulban, O.F., 2021. LayNii: a software suite for layer-fMRI. Neuroimage 237, 118091. doi:10.1016/j.neuroimage.2021.118091.

Huber, L., Finn, E.S., Chai, Y., Goebel, R., Stirnberg, R., Stöcker, T., Marrett, S., Uludag, K., Kim, S.G., Han, S., Bandettini, P.A., Poser, B.A., 2020. Layer-dependent functional connectivity methods. Prog. Neurobiol. 101835. doi:10.1016/j.pneurobio.2020.101835.

Huber, L., Goense, J., Kennerley, A.J., Ivanov, D., Krieger, S.N., Lepsien, J., Trampel, R., Turner, R., Möller, H.E., 2014. Investigation of the neurovascular coupling in positive and negative BOLD responses in human brain at 7T. Neuroimage 97, 349–362. doi:10.1016/j.neuroimage.2014.04.022.

Huber, L., Handwerker, D.A., Jangraw, D.C., Chen, G., Hall, A., Stüber, C., Gonzalez-Castillo, J., Ivanov, D., Marrett, S., Guidi, M., Goense, J., Poser, B.A., Bandettini, P.A., 2017. High-resolution CBV-fMRI allows mapping of laminar activity and connectivity of cortical input and output in human M1. Neuron 96, 1253–1263. doi:10.1016/j.neuron.2017.11.005.

Huber, L., Ivanov, D., Guidi, M., Turner, R., Uludağ, K., Möller, H.E., Poser, B.A., 2016. Functional cerebral blood volume mapping with simultaneous multi-slice acquisition. Neuroimage 125, 1159–1168. doi:10.1016/j.neuroimage.2015.10.082.

Jenkinson, M., Beckmann, C.F., Behrens, T.E.J., Woolrich, M.W., Smith, S.M., 2012. FSL–Review. Neuroimage 62, 782–790. doi:10.1016/j.neuroimage.2011.09.015.

Jordan, R., Keller, G.B., 2020. Opposing Influence of top-down and bottom-up input on excitatory layer 2/3 neurons in mouse primary visual cortex. Neuron 108. doi:10.1016/j.neuron.2020.09.024, 1194-1206.e5.

Kachergis, G., Wyatte, D., O'Reilly, R.C., de Kleijn, R., Hommel, B., 2014. A continuous time neural model for sequential action. Philos. Trans. R. Soc. B 1–8. doi:10.1098/rstb.2013.0623.

Kanai, R., Komura, Y., Shipp, S., Friston, K., 2015a. Cerebral hierarchies: predictive processing, precision and the pulvinar. Philos. Trans. R. Soc. B Biol. Sci. 370. doi:10.1098/rstb.2014.0169.

Kanai, R., Komura, Y., Shipp, S., Friston, K., 2015b. Cerebral hierarchies: predictive processing, precision and the pulvinar. Philos. Trans. R. Soc. B Biol. Sci. 370. doi:10.1098/rstb.2014.0169.

Keller, G.B., Mrsic-Flogel, T.D., 2018. Predictive processing: a canonical cortical computation. Neuron 100, 424–435. doi:10.1016/j.neuron.2018.10.003.

Klein, R., Ivanoff, J., 2000. Inhibition of return. Trends Cogn. Sci. 4, 138–147. doi:10.4249/scholarpedia.3650.

Lawrence, S.J.D., van Mourik, T., Kok, P., Koopmans, P.J., Norris, D.G., de Lange, F.P., 2018. Laminar organization of working memory signals in human visual cortex. Curr. Biol. 28, 3435–3440. doi:10.1016/j.cub.2018.08.043.

Lee, T.S., Mumford, D., 2003. Hierarchical Bayesian inference in the visual cortex. J. Opt. Soc. Am. A 20, 1434–1448.

Lu, H., Golay, X., Pekar, J.J., Van Zijl, P.C.M., 2003. Functional magnetic resonance imaging based on changes in vascular space occupancy. Magn. Reson. Med. 50, 263–274. doi:10.1002/mrm.10519.

Manita, S., Suzuki, T., Homma, C., Matsumoto, T., Odagawa, M., Yamada, K., Ota, K., Matsubara, C., Inutsuka, A., Sato, M., Ohkura, M., Yamanaka, A., Yanagawa, Y., Nakai, J., Hayashi, Y., Larkum, M.E., Murayama, M., 2015. A top-down cortical circuit for accurate sensory perception. Neuron 86, 1304–1316. doi:10.1016/j.neuron.2015.05.006.

Mease, R.A., Krieger, P., Groh, A., 2014. Cortical control of adaptation and sensory relay mode in the thalamus. Proc. Natl. Acad. Sci. USA 111, 6798–6803. doi:10.1073/pnas.1318665111.

Mumford, D., 1992. On the computational architecture of the neocortex. Biol. Cybern. 66, 241–251. doi:10.1007/BF00198477.

Nobre, A.C., Van Ede, F., 2018. Anticipated moments: temporal structure in attention. Nat. Rev. Neurosci. doi:10.1038/nrn.2017.141.

O'Connor, D.H., Peron, S.P., Huber, D., Svoboda, K., 2010. Neural activity in barrel cortex underlying vibrissa-based object localization in mice. Neuron 67, 1048–1061. doi:10.1016/j.neuron.2010.08.026.

Pluta, S., Naka, A., Veit, J., Telian, G., Yao, L., Hakim, R., Taylor, D., Adesnik, H., 2015. A direct translaminar inhibitory circuit tunes cortical output. Nat. Neurosci. 18, 1631–1640. doi:10.1038/nn.4123.

Pluta, S.R., Telian, G.I., Naka, A., Adesnik, H., 2019. Superficial layers suppress the deep layers to fine-tune cortical coding. J. Neurosci. 39, 2052–2064. doi:10.1523/JNEUROSCI.1459-18.2018.

Poser, B.A., Koopmans, P.J., Witzel, T., Wald, L.L., Barth, M., 2010. Three dimensional echo-planar imaging at 7 Tesla. Neuroimage 51, 261–266. doi:10.1016/j.neuroimage.2010.01.108.

Quiquempoix, M., Fayad, S.L., Boutourlinsky, K., Leresche, N., Lambert, R.C., Bessaih, T., 2018. Layer 2/3 pyramidal neurons control the gain of cortical output. Cell Rep. 24. doi:10.1016/j.celrep.2018.08.038, 2799–2807.e4.

R Core Team, 2013. R: A language and Environment for Statistical Computing. R Foundation for Statistical Computing doi:10.1007/978-3-540-74686-7.

Rao, R.P.N., Ballard, D.H., 1999. Predictive coding in the visual cortex: a functional interpretation of some extra-classical receptive-field effects. Nat. Neurosci. 2, 79–87. doi:10.1038/4580.

Reed, J.L., Qi, H.-X., Kaas, J.H., 2011. Spatiotemporal properties of neuron response suppression in owl monkey primary somatosensory cortex when stimuli are presented to both hands. J. Neurosci. 31, 3589–3601. doi:10.1523/JNEUROSCI.4310-10.2011.

Reed, J.L., Qi, H.X., Zhou, Z., Bernard, M.R., Burish, M.J., Bonds, A.B., Kaas, J.H., 2010. Response properties of neurons in primary somatosensory cortex of owl monkeys reflect widespread spatiotemporal integration. J. Neurophysiol. 103, 2139–2157. doi:10.1152/jn.00709.2009.

Roelfsema, P.R., Holtmaat, A., 2018. Control of synaptic plasticity in deep cortical networks. Nat. Rev. Neurosci. 19, 166–180. doi:10.1038/nrn.2018.6.

Self, M.W., van Kerkoerle, T., Goebel, R., Roelfsema, P.R., 2019. Benchmarking laminar fMRI: neuronal spiking and synaptic activity during top-down and bottom-up processing in the different layers of cortex. Neuroimage 197, 806–817. doi:10.1016/j.neuroimage.2017.06.045.

Shipp, S., Adams, R.A., Friston, K.J., 2013. Reflections on agranular architecture: predictive coding in the motor cortex. Trends Neurosci. doi:10.1016/j.tins.2013.09.004.

Slater, B.J., Sons, S.K., Yudintsev, G., Lee, C.M., Llano, D.A., 2019. Thalamocortical and intracortical inputs differentiate layer-specific mouse auditory corticocollicular neurons. J. Neurosci. 39, 256–270. doi:10.1523/JNEUROSCI.3352-17.2018.

Thomson, A.M., 2007. Functional maps of neocortical local circuitry. Front. Neurosci. 1, 19–42. doi:10.3389/neuro.01.1.1.002.2007.

Turner, R., De Haan, D., 2017. Bridging the gap between system and cell: the role of ultra-high field MRI in human neuroscience. In: Tara, M., Sam, M., Nikolas, R. (Eds.), Vital Models The Making and Use of Models in the Brain Sciences. Elsevier B.V., pp. 179–220. doi:10.1016/bs.pbr.2017.05.005.

Uludağ, K., Blinder, P., 2018. Linking brain vascular physiology to hemodynamic response in ultra-high field MRI. Neuroimage 168, 279–295. doi:10.1016/j.neuroimage.2017.02.063.

Waehnert, M.D., Dinse, J., Weiss, M., Streicher, M.N., Waehnert, P., Geyer, S., Turner, R., Bazin, P.L., 2014. Anatomically motivated modeling of cortical laminae. Neuroimage 93, 210–220. doi:10.1016/j.neuroimage.2013.03.078.

Yang, J., Fukunaga, M., Yu, Y., Huber, L., Bandettini, P.A., Sadato, N., 2021a. Layer-specific activation of prediction in the human midcingulate cortex. Proc. Intl. Soc. Mag. Reson. Med. 29, 3369.

Yang, J., Huber, L., Yu, Y., Bandettini, P.A., 2021b. Linking cortical circuit models to human cognition with laminar fMRI. Neurosci. Biobehav. Rev. 128, 467–478. doi:10.1016/j.neubiorev.2021.07.005.

Yu, Y., Huber, L., Yang, J., Jangraw, D.C., Handwerker, D.A., Molfese, P.J., Chen, G., Ejima, Y., Wu, J., Bandettini, P.A., 2019. Layer-specific activation of sensory input and predictive feedback in the human primary somatosensory cortex. Sci. Adv. 5, eaav9053. doi:10.1126/sciadv.aav9053.